

# New sector morphologies emerge from anisotropic colony growth

Daniel W. Swartz, Hyunseok Lee, and Mehran Kardar

*Department of Physics, Massachusetts Institute of Technology, Cambridge, Massachusetts 02139, USA*

Kirill S. Korolev

*Department of Physics, Graduate Program in Bioinformatics and Biological Design Center,  
Boston University, Boston, Massachusetts 02215, USA*

(Dated: May 31, 2024)

Competition during range expansions is of great interest from both practical and theoretical view points. Experimentally, range expansions are often studied in homogeneous Petri dishes, which lack spatial anisotropy that might be present in realistic populations. Here, we analyze a model of anisotropic growth, based on coupled Kardar-Parisi-Zhang and Fisher-Kolmogorov-Petrovsky-Piskunov equations that describe surface growth and lateral competition. Compared to a previous study of isotropic growth, anisotropy relaxes a constraint between parameters of the model. We completely characterize spatial patterns and invasion velocities in this generalized model. In particular, we find that strong anisotropy results in a distinct morphology of spatial invasion with a kink in the displaced strain ahead of the boundary between the strains. This morphology of the out-competed strain is similar to a shock wave and serves as a signature of anisotropic growth.

## INTRODUCTION

Surface growth appears in diverse contexts such as molecular beam epitaxy, flame propagation, imbibing, and many others [1–3]. Growth patterns are also relevant to ecology and evolution as they describe population dynamics in epidemics, ecological succession, and the spreading of a biofilm or a cancerous tumor [4]. These biological examples may harbor an extra layer of complexity when distinct subpopulations compete with each other during spatial range expansion. Therefore, there is substantial interest in understanding and potentially exploiting the intricate interplay of spatial population growth and competition. [5–9]

Simplified models of growing colonies, such as the Eden and stepping stone models [10, 11] focus on the reproduction at the edge of the expanding colony, assuming that the cells left behind in bulk do not grow. Starting from a flat initial line of cells, the fluctuating growing surface can then be described mathematically by the Kardar-Parisi-Zhang (KPZ) equation [12], a classic model of surface growth. On the other hand, competition of two strains on a flat substrate can be modelled by the Fisher-Kolmogorov-Petrovsky-Piskunov (FKPP) equation [13, 14], a classic model for reaction-diffusion waves. Reference [15] proposed the minimal couplings between KPZ and FKPP equations to describe the competition of several species during range expansion. In further work, we employed these equations to describe possible morphologies and invasion speeds for isotropic growth of two competing species. [16]

While the above models are of inherent mathematical interest, their empirical motivation comes primarily from experiments with microbial colonies grown on standard agar plates. In such experiments, two stains with different properties are mixed together (often in unequal

ratios), and a small drop of the inoculant is deposited on a Petri dish. If the minority strain is somehow more “fit,” its relative frequency will increase with time, and it will produce a spatial domain, termed a sector, with a characteristic morphology. The most common morphology is a protruding bulge signifying the faster expansion rate of the minority strain [17], but other morphologies have also been observed [8]. Our model of coupled KPZ and FKPP equations successfully reproduced these morphologies and predicted how various aspects of sector shapes depend on microscopic parameters. [16]

In this paper, we aim to relax one of the key assumptions of our previous work: the isotropy of space. Spatial growth can be anisotropic for a large number of reasons: temperature and precipitation gradients, magnetotaxis, substrate patterns such as the preferred orientation of collagen fibers, gradients of chemo-attractants, or fluid flow [4, 7, 18–21]. We note that, apart from trivial changes, which can be removed by a simple change of variables, spatial anisotropy does not produce any new terms in the equations, but relaxes a constraint between two parameters. The ratio of these parameters can then be regarded as a measure of anisotropy. We find that weak anisotropy leads only to quantitative changes in the dynamics, but that once the parameter ratio exceeds a certain threshold, a new sector morphology appears. This morphology is characterized by a “shock” wave spreading ahead of the sector established by the fitter strain. We present a complete analytical picture of anisotropic growth and confirm our results with simulations.

## MODEL

### Thin edge approximation

In many contexts, two dimensional growth of a colony on a substrate is effectively limited to a thin region at the population edge because of nutrient limitations [22, 23], buildup of pressure [22, 24, 25], or other factors. As a result, the state of the population can be described by two effectively one-dimensional variables: the position of the front,  $h$ , and the relative fraction of the genotype of interest,  $f$ . Both variables depend on time  $t$  and location along the population edge  $x$ . For simplicity, we consider nearly planar fronts without overhangs, so that  $x$  uniquely specifies a point on a growing front. The whole two-dimensional structure of the population can then be reconstructed from  $h(t, x)$  and  $f(t, x)$ . This is particularly easy for microbial colonies because there are no population dynamics behind the front, and the population is frozen in the state it had when the growth front passed this spatial location.

To make a dynamical model that depends only on  $f$  and  $h$ , we need to further assume that the growth and competition depend only on the local state of the population. For example, we need to limit our analysis to growth conditions with plentiful nutrients; otherwise, the growth would be affected by the spatial distribution of the nutrients, which is not included in this modeling framework.

The FKPP equation [13, 14, 26–28] provides a good starting point to describe the invasion of a fitter mutant with relative abundance  $f(t, x)$ , which is initially confined to a small spatial domain

$$\frac{\partial f}{\partial t} = sf(1 - f) + D_f \frac{\partial^2 f}{\partial x^2}. \quad (1)$$

This equation is the default model for strictly one-dimensional populations, e.g. inside a channel, and it should be applicable to perfectly flat fronts. The key prediction of the FKPP equation is that the fitter mutant is first established locally (i.e.  $f$  saturates to  $f = 1$  in small spatial domain) and then spreads outward with velocity  $u_0 = 2\sqrt{sD_f}$ .

In turn, the dynamics of  $h$  is described by the KPZ equation [12], which for a genetically homogeneous colony, say with  $f = 0$ , takes the form

$$\frac{\partial h}{\partial t} = v + \frac{\lambda}{2} \left( \frac{\partial h}{\partial x} \right)^2 + D_h \frac{\partial^2 h}{\partial x^2}. \quad (2)$$

Here,  $v$  is the expansion speed of a flat front and  $D_h$  describes the relaxation of front undulations due to the dependence of the expansion velocity on the local curvature. [23] The remaining parameter  $\lambda$  is described below.

### Effects of anisotropy

To understand the origin of  $\lambda$  and the nature of the coupling between the KPZ and FKPP equations consider the dynamics of a sector boundary in Fig. 1. We first consider the case of isotropic growth, where two identical (i.e. neutral) strains grow outward with velocity  $v$ . The population front makes an angle  $\theta$  with respect to a horizontal line,  $h = \text{const}$ . During a time interval  $dt$ , the increment of height  $dh$  equals  $v dt / \cos \theta$ , while the demarcation point between the strains drifts by  $dx_b = v dt \sin(\theta)$ . In the limit of small slope, this leads to

$$\frac{dh}{dt} = v \left( 1 + \frac{\theta^2}{2} \right), \quad \text{and} \quad \frac{dx_b}{dt} = v\theta. \quad (3)$$

We then use  $\theta \approx -\partial h / \partial x$  and obtain the KPZ equation with  $\lambda = v$  and an additional drift term for the FKPP equation

$$u_{\text{drift}}(\theta) = -v\theta \frac{\partial f}{\partial x} = v \frac{\partial f}{\partial x} \frac{\partial h}{\partial x}. \quad (4)$$

Upon further accounting for the dependence of  $v$  on  $f$  via  $v(f) \approx v_0 + \alpha f$ , we obtain the two coupled equations studied in our previous work Ref. [16].

In the case of anisotropic growth, as in the second panel of Fig. 1, the front velocity  $v$  can depend of the heading angle  $\theta$ . Also, the sector boundary is not necessarily perpendicular to the expansion front, instead offset by some amount  $\epsilon$  which should depend on  $\theta$ . We now proceed to account for anisotropy by including the effects of both  $\epsilon(\theta)$  and  $v(\theta)$ . In a typical bi-axial anisotropy, an initially circular seed will grow into a lozenge shape [29], with the largest facet proceeding along the direction of the *slowest growth*. We choose the direction of slowest growth to define  $\theta = 0$ . The growing colony should be symmetric to flips about the vertical axis,  $(x, \theta, \epsilon) \rightarrow (-x, -\theta, -\epsilon)$ , implying that  $v(\theta)$  should be even in  $\theta$  while  $\epsilon(\theta)$  should be odd. We can then expand  $v(\theta)$  around this slowest direction as  $v(\theta) = v(0) + v''(0)\theta^2/2 + \dots$ , and obtain the new set of equations with coefficients that will now depend on  $v''(0)$  and  $\epsilon'(0)$ . This results in

$$\frac{\partial h}{\partial t} = v_0 + \alpha f + \frac{\lambda}{2} \left( \frac{\partial h}{\partial x} \right)^2 + D_h \frac{\partial^2 h}{\partial x^2}, \quad (5)$$

with  $\lambda = v_0 + v''$  and

$$\frac{\partial f}{\partial t} = s_0 f(1 - f) + D_f \frac{\partial^2 f}{\partial x^2} + \beta \frac{\partial h}{\partial x} \frac{\partial f}{\partial x}, \quad (6)$$

with  $\beta = v_0(1 + \epsilon'(0))$ . Note that isotropic growth requires  $\lambda = \beta = v_0$ . This condition might also hold for some anisotropic growth scenarios with  $v''(0) = v_0\epsilon'(0)$ .

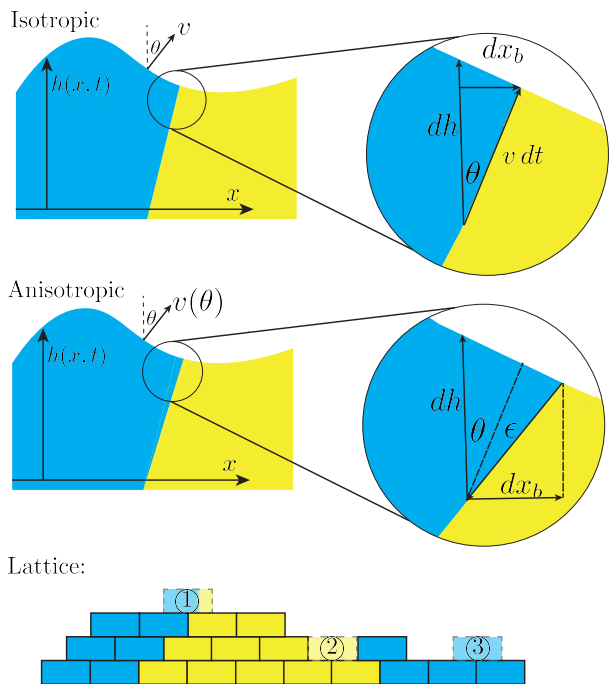


FIG. 1. **Colony growth can be described by a height function  $h(t, x)$  and population composition  $f(t, x)$**  (Color Online). The top panel shows two neutral strains (blue and yellow) with the same expansion speed growing under isotropic conditions. The second panel shows the case of neutral expansion with speed  $v(\theta)$ , which can depend on the direction of growth specified by the angle  $\theta$ . In general, the boundary between the strains is not orthogonal to the growth front and forms an angle  $\epsilon(\theta)$  with the front normal. The vertical growth  $dh$ , and horizontal drift  $dx_b$  during time  $dt$  depend on the slope  $\theta$  leading to the nonlinearities in Eqs. (5) and (6). The bottom panel illustrates a discrete growth model, which avoids overhangs by allowing new growth only when both lower sites are occupied. Even the simplest implementation of this so-called solid-on-solid model produces anisotropic growth. The numbers 1, 2, and 3 refer to distinct possibilities that affect how the color of the newly occupied site is determined; see main text.

A trivial example of anisotropic growth where  $\beta = \lambda$  is the spread of a two-dimensional reaction-diffusion wave where the coordinates  $x$  and  $y$  have been scaled differently. Generically,  $\lambda \neq \beta$ , and we will describe the degree of anisotropy by  $\beta/\lambda$  in the following.

Previous works have coupled Eqs. (1) and (2) to study the extinction transition coupled to a growing surface [15, 30, 31]. The dynamical equations were proposed using a gradient expansion in powers of  $\partial_x h$  and expanding further around  $f = 0$  in the vicinity of extinction. Equations (1) and (2) are readily generalized by allowing parameters  $v, s, \lambda, D_f, D_h$  to depend on either  $f$  and  $\partial_x h$ . Expanding in powers of the gradient should generate many higher-order terms which are neglected. The additional term  $\beta_1 \partial_x f \partial_x h$  which causes the sector bound-

ary to drift should also be included at this order in the gradient expansion. The expansion of the selection coefficient  $s$  will generate several terms at lowest order. The first few are [15]

$$s = s_0 + \beta_2 \partial_x^2 h + c/2 (\partial_x h)^2 + \dots$$

Isotropic growth is equivalent to demanding that the equations for  $f$  and  $h$  are invariant to Galilean (rotational) transformations [15], which is satisfied for  $\beta_1 = \lambda$  and  $c = 0$ . For simplicity, we neglect the feedback of the front curvature on the selection coefficient, setting  $\beta_2 = 0$ . We consider the effects of anisotropy generated by relaxing the constraint on  $\beta_1$  (which we will from here on call  $\beta$ ). While anisotropy is also generated for  $c \neq 0$ , there is currently no demonstrated example of selection depending on the slope of the front.

### Lattice Implementation

As a concrete example of anisotropic growth, we consider the so-called solid-on-solid model on a triangular lattice; see Ref. [15] and Fig. 1. At each time step, a potential growth site is selected, above two sites that are already occupied (thus excluding overhangs). The identity of the new cell is then based on the identities of the two ancestors below, see sites labeled 1, 2, 3 in Fig. 1. If both ancestors are yellow, then a new yellow cell is added with probability  $1 - p_y$ . If both ancestors are blue, then a new blue cell is added with probability  $1 - p_b$ . If one ancestor is yellow and the other is blue, a new cell is added with probability  $1 - (p_b + p_y)/2$ . The color of this child cell is blue with probability  $(1 + s/2)$  and yellow otherwise.

The parameters  $p_y$  and  $p_b$  determine the effective growth rates of the strains and can be related to  $v_0$  and  $\alpha$  in Eq. (5). The other parameter  $s$  describes the effect of local competition and is related to  $s_0$  in Eq. (6). Typical spatial patterns produced by this model are shown in Fig 2.

### Related Models

The proposed equations are closely related to population dynamics in a flowing fluid [7, 32, 33]. This is easy to see after a change of variables from  $h$  to a velocity field  $w$  defined as  $w = -\lambda \partial h / \partial x$  because the KPZ equation transforms into a one-dimensional Burgers equation of fluid dynamics:

$$\frac{\partial w}{\partial t} + w \frac{\partial w}{\partial x} = -\alpha \lambda \frac{\partial f}{\partial x} + D_h \frac{\partial^2 w}{\partial x^2}, \quad (7)$$

$$\frac{\partial f}{\partial t} + \frac{\beta w}{\lambda} \frac{\partial f}{\partial x} = s_0 f(1 - f) + D_f \frac{\partial^2 f}{\partial x^2}. \quad (8)$$

Note that the coupling term in the FKPP equation now has a very straightforward interpretation. The fraction of the mutant  $f$  is advected along the flow. For isotropic growth ( $\beta/\lambda = 1$ ), the advection velocity is the flow velocity. More generally, however, the advection velocity can be either greater or slower than the fluid flow [34] due to active motility (e.g. chemotaxis) or interactions with the substrate. Other notable changes in the equations are (i) that  $D_h$  represents fluid viscosity, (ii) that  $\alpha\lambda f$  represents the  $f$ -dependent component of the mechanical pressure due to growth or other factors [22, 35], and (iii) the KPZ nonlinearity turns into the nonlinear part in the material derivative.

Equations (5) and (6) can also be used to study the case of colony erosion, where the front recedes and the velocity  $v$  is negative. Starting from Eqs. (5) and (6) and taking  $h \rightarrow -h$ , we find the corresponding model for colony erosion

$$\frac{\partial f}{\partial t} = s_0 f(1 - f) + D_f \frac{\partial^2 f}{\partial x^2} + \beta \frac{\partial h}{\partial x} \frac{\partial f}{\partial x}, \quad (9)$$

$$\frac{\partial h}{\partial t} = -v_0 - \alpha f - \frac{\lambda}{2} \left( \frac{\partial h}{\partial x} \right)^2 + D_h \frac{\partial^2 h}{\partial x^2}, \quad (10)$$

which has the same form as Eqs. (5) and (6), but with a flipped sign for  $v_0$ ,  $\alpha$ ,  $\lambda$ , and  $\beta$ . Thus, we can take advantage of the  $h \rightarrow -h$  transformation to fix the sign of one of these four parameters. We chose to set  $\lambda > 0$  in our analysis, hence our results need to be transformed accordingly before comparing to the models with negative  $\lambda$ . In particular, this applies to the solid-on-solid stochastic cellular automaton model shown in Figs. 1 and 2, which has  $\lambda < 0$  due to the restriction that both lower sites must be occupied for a growth event to occur.

Equations (5) and (6) can be further simplified by removing the constant term  $v_0$  by changing variable from  $h$  to  $h + v_0 t$  and setting  $s_0$  to be positive. The latter can be accomplished by changing  $f$  to  $1 - f$  if  $s_0 < 0$ . This leaves only the signs of  $\alpha$  and  $\beta$  to be undefined. In the following, we will explore both positive and negative  $\alpha$ , but will limit our discussion to  $\beta > 0$ . The dynamics with negative  $\beta$  are sufficiently different to warrant a separate exposition.

## RESULTS

### Morphologies

In previous work [16], using a combination of numerical and analytical techniques, we demonstrated that Eqs. (5) and (6) can reproduce known sector morphologies [16] for  $\lambda = \beta$ . The morphologies present in this isotropic limit are a V-shaped dent, a composite bulge, and a circular arc. The V-shaped dent and circular arc have been observed experimentally [8, 17], and the composite bulge

was previously predicted using a construction akin to geometric optics for light propagation [8]. Our analysis in Ref. [16] further clarified the origins of these morphologies and determined the invasion speed of the mutant as a function of microscopic parameters such as  $\alpha$  and  $s_0$ .

Here, we generalize our analysis to anisotropic growth and determine how morphologies and invasion velocities are affected by  $\beta/\lambda$ . The main results are summarized in Fig. 2, which shows how morphologies change with the expansion rate difference  $\alpha$  between the blue and yellow strains. As  $\alpha$  increases from negative to positive values, the morphology transitions from a *V-shaped dent* to a *composite bulge* and then a *circular arc*. These transition are present for both isotropic and anisotropic growth, but a qualitatively new morphology emerges above a critical ratio of  $\beta/\lambda$  for a sufficiently large  $\alpha$ ; see the last panel in Fig. 2. This new morphology, which we call an *escaping bulge*, is fundamentally different from the other three types of sectors because the boundary between the blue and yellow strains is preceded by a deformation in the colony shape deep in the domain occupied by a less fit strain. In the following, we completely characterize this new morphology and determine the invasion speeds of the strain boundary and the deformation. We also obtain the effects of anisotropy on the invasion velocity for the V-shaped dent, composite bulge, and circular arc.

### Invasion speed: Pulled Waves

The key observable predicted by Eqs. (5) and (6) is the invasion velocity  $u$ , i.e. the velocity with which the fitter (yellow) strain displaces the other (blue) strain along the front. By common convention, we take  $u$  to be positive for a right-moving wave. In this section, we compute  $u$  from a travelling-wave solution to Eqs. (5) and (6) for all morphologies. Note that the FKPP equation in Eq. (6) describes a *pulled wave*, dominated by the dynamics at small  $f$  [28]. The opposite case of *pushed waves* is analyzed in the next section.

We begin by recalling two relevant velocities in Eqs. (5) and (6). The first velocity is the Fisher speed  $u_0 = 2\sqrt{s_0 D_f}$ , which is the speed of a pulled wave in the absence of the coupling to  $h$  [13, 14]. For example, when  $\alpha = 0$ , the expanding profile is flat ( $\partial_x h = 0$ ), and the invasion speed must equal to the Fisher speed. The second velocity is the natural speed of invasion for the circular arc morphology, which emerges entirely from the KPZ equation  $u_{\text{kpz}} = \sqrt{2\alpha\lambda}$ ; see Ref. [16].

Previously, we demonstrated that the invasion speed of an isotropic pulled wave is given by the largest of these two velocities for any  $\alpha$  [16]. This conclusion persists for anisotropic growth until  $\alpha$  exceeds a critical value, and the front shape switches to an escaping bulge morphology (Fig. 3). After this transition, the invasion speed falls below  $u_{\text{kpz}}$ , but stays above the Fisher velocity.

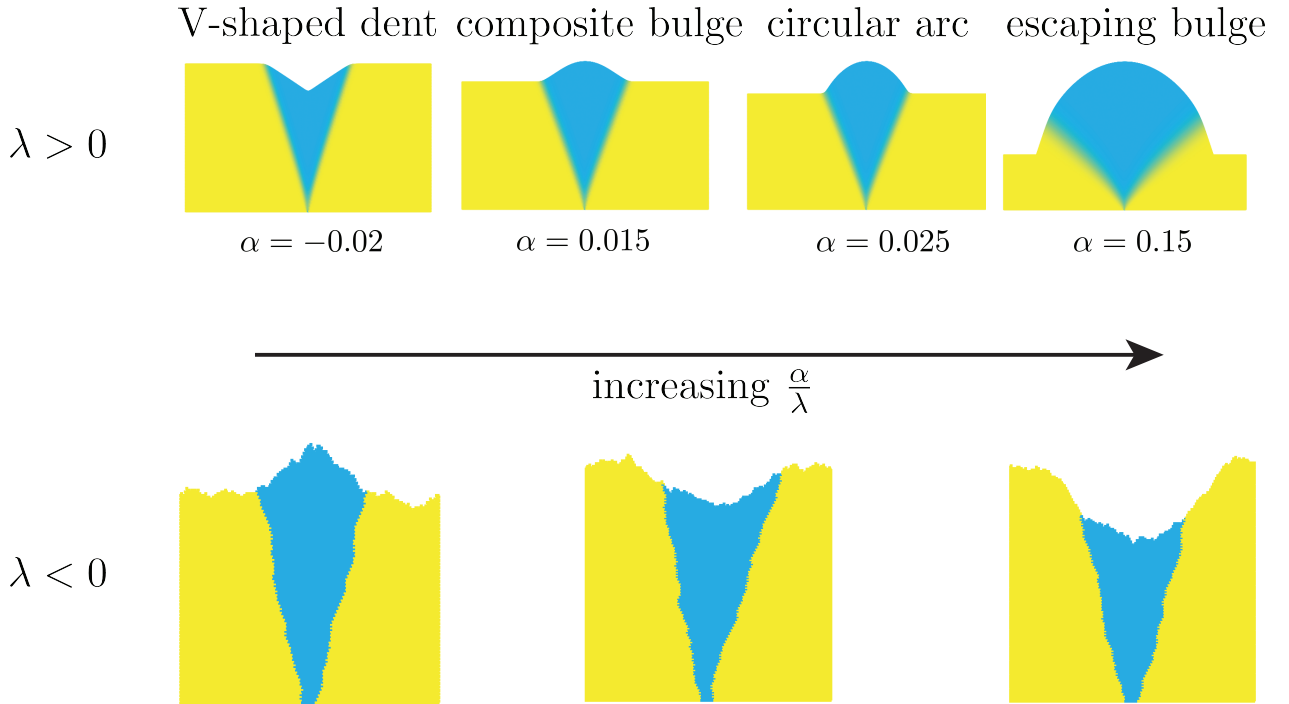


FIG. 2. **Anisotropy allows for an “Escaping Bulge” sector morphology** (Color Online). The top panel shows morphologies that we observed in numerical solutions of deterministic Eqs. (5) and (6). To the left (at negative  $\alpha$ ) is a V-shaped dent with straight edges. Next, at small positive  $\alpha$ , is the composite bulge morphology, again with constant limiting slopes around a circular arc in the middle. At larger  $\alpha$  the sector shape is a pure circular arc, commonly observed in the experiments. The final shape is the new morphology termed ‘escaping bulge’. This shape requires large  $\alpha$ , but, more importantly, it can only be attained in the presence of large anisotropy ( $\lambda \geq 2\beta$  for pulled waves). The bottom panel shows that similar results hold in stochastic numerical simulations; see Fig. 1. Previous work has shown that this solid-on-solid lattice model has a negative  $\lambda$ , so, to compare to the top panel, one needs to transform  $(h, \beta, \alpha) \rightarrow (-h, -\beta, -\alpha)$ . With this transformation in mind, the left image corresponds to the V-shaped dent, and the right image to the escaping bulge (note that the sector boundary is within a tilted region). The middle image corresponds to either the composite bulge or the circular arc. To distinguish the two, we would need to run simulations at much larger system sizes. For the top row of figures the parameters are  $D_f = 1$ ,  $D_h = 1$ ,  $v_0 = 0.08$ ,  $\lambda = 20$ ,  $s_0 = 0.25$ , and  $\beta = 5$ . For the bottom row the parameters of the lattice model are, from left to right,  $(p_b, p_y, s)$  equals  $(0, 0.3, 0.5)$ ,  $(0.17, 0.3, 0.5)$ , and  $(0.3, 0, 0.5)$ .

To compute the invasion speed for the escaping bulge morphology, we switch to a reference frame co-moving with the sector boundary in both horizontal and vertical directions. The horizontal velocity  $u$  can be eliminated via a change of variable:  $z = x - ut$ . The vertical position of the sector boundary can be determined as follows. The inner region of the escaping bulge contains a single strain and, therefore, should be a self-similar solution of the KPZ equation, i.e. a line or a parabola [16]. Given the bulge geometry, we conclude that the inner region is described by  $h(x, t) \approx (v_0 + \alpha)t - x^2/(2\lambda t)$ , which extends until the sector boundary is reached at  $x = \pm ut$ . Upon eliminating  $x$  from these two equations, we find that the boundary is located at  $h = (v_0 + \alpha - u^2/(2\lambda))t$ . We then redefine  $h$  as  $h + (v_0 + \alpha - u^2/(2\lambda))t$ , and obtain the

following set of equations

$$-uf' = s_0 f(1-f) + D_f f'' + \beta f' h', \quad (11)$$

$$-uh' = \frac{u^2}{2\lambda} + \alpha(f-1) + \frac{\lambda}{2}(h')^2 + D_h h'', \quad (12)$$

where the derivatives are with respect to  $z$ . The invasion velocity  $u$  is then determined by seeking a nontrivial stationary solution to the equations above.

Since the velocity of pulled waves is controlled by the region with vanishing  $f$ , we need to analyze the behavior of  $h$  at  $z \rightarrow +\infty$ . From Eq. (12), it immediately follows that

$$h'(z \rightarrow +\infty) = -\frac{u}{\lambda} - \frac{\sqrt{2\alpha\lambda}}{\lambda} \quad (13)$$

because  $f(z \rightarrow +\infty) = 0$  and  $h''$  vanishes for a constant slope.

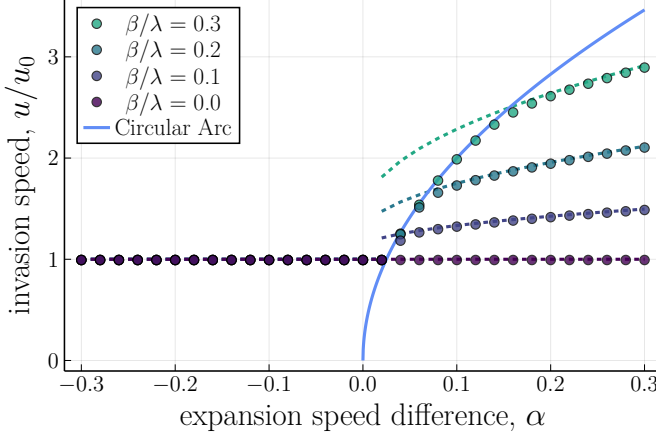


FIG. 3. **Three regimes for anisotropic pulled waves** (Color Online). The mutant can invade with the Fisher velocity, the velocity of the circular arc  $u_{\text{kpz}} = \sqrt{2\alpha\lambda}$  (solid line), or the escaping bulge velocity predicted by Eq. (14) (dashed lines) depending on the expansion speed difference  $\alpha$  and the degree of anisotropy  $\beta/\lambda$ . The dots are obtained from numerical solutions of Eqs. (5) and (6). Parameters are:  $v_0 = 1$ ,  $\lambda = 20$ ,  $D_h = 1$ ,  $D_f = 1$ , and  $s_0 = 0.25$ .

Equation (11) then reduces to a regular FKPP equation in a comoving reference frame with an additional drift velocity  $-\beta h'(z \rightarrow +\infty)$  given by Eq. (13). Thus,  $u = 2\sqrt{s_0 D_f} + \beta(u/\lambda + \sqrt{2\alpha\lambda}/\lambda)$ , which simplifies to

$$u = \frac{2\sqrt{s_0 D_f} + \frac{\beta}{\lambda}\sqrt{2\alpha\lambda}}{1 - \beta/\lambda}. \quad (14)$$

This solution agrees with the simulations for appropriate values of the parameters shown in Fig. 3, but it clearly diverges for  $\beta = \lambda$  and, in general, is valid only in the regime when the escaping bulge is observed. We can determine this region of applicability by considering the vertical velocity of the sector boundary which we determined above to be  $v_0 + \alpha - u^2/(2\lambda)$ . This velocity must be larger than the upward velocity of the flat front  $v_0$  in order for an escaping bulge to persist at long times. Thus, an escaping bulge is only possible when  $u < \sqrt{2\alpha\lambda}$ , i.e.  $u < u_{\text{kpz}}$ . From Eq. (14), it then follows that the escaping bulge is only possible for  $\beta < \lambda/2$ . In other words, the degree of anisotropy must exceed a critical value for the escaping bulge to occur. We illustrate the transitions among all the possible regimes in Fig. 4.

Another important aspect of the escaping bulge morphology is a shock-like singularity ahead of the sector boundary. The speed of this singularity  $c$  is greater than  $u$  and can be computed by finding the intersection point between the unperturbed front of the blue strain, which moves up with velocity  $v_0$ , and the straight slope extending downward from the sector boundary. Since we have determined both the value of this slope and the location of the sector boundary, we can immediately find

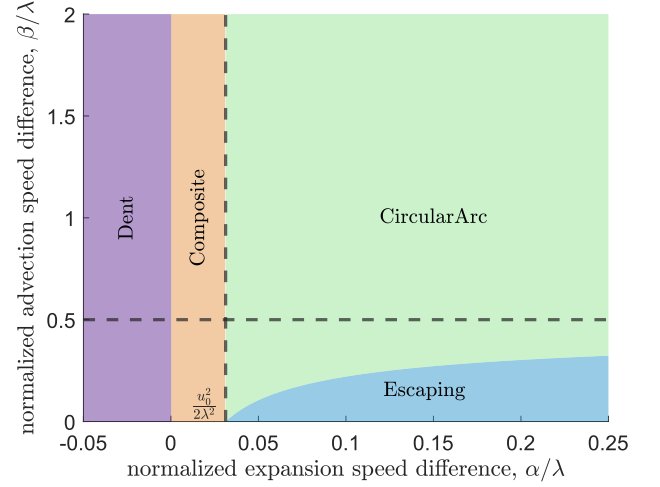


FIG. 4. **Predicted phase diagram of morphologies for pulled waves based on Eqs. (5) and (6)** (Color Online). The isotropic case is located along the line  $\beta/\lambda = 1$  (not shown). Note that small anisotropy does not lead to new morphologies, and the escaping bulge exists only for  $\beta/\lambda < 1/2$  (horizontal dashed line). Parameters not shown are  $u_0 = 1$  and  $\lambda = 10$ .

that

$$c = \frac{1}{2}(u + \sqrt{2\alpha\lambda}). \quad (15)$$

This result is confirmed by simulations in Fig. 5 and further supports the conclusion that as escaping bulge is only possible when  $u < u_{\text{kpz}}$  because the exact same condition is required to ensure that the singularity is indeed ahead of the sector boundary, i.e.  $c > u$ .

### Invasion speed: Pushed Waves

The FKPP equation considered so far is a special case of a larger class of equations with  $s_0$  replaced by an arbitrary function  $s(f)$ . This generalization reflects frequency-dependent selection, which frequently arises due to metabolite exchanges or other forms of collective or cooperative growth strategies [36–41]. Although our analysis can be applied to any  $s(f)$ , we will restrict our discussion to  $s(f) = s_0(f - f_0)$  with  $s_0 > 0$ , which captures all possible scenarios with minimal additional complexity. Furthermore, we can take advantage of the exact analytical solutions of the generalized FKPP equation with this linear form of  $s(f)$ . Thus, we now replace Eq. (6) by

$$\frac{\partial f}{\partial t} = s_0(f - f_0)f(1 - f) + D_f \frac{\partial^2 f}{\partial x^2} + \beta \frac{\partial h}{\partial x} \frac{\partial f}{\partial x}, \quad (16)$$

while keeping Eq. (5) the same.

For  $f_0 < -1/2$ , the solution of the generalized FKPP equation (without the coupling to  $h$ ) is a pulled wave,

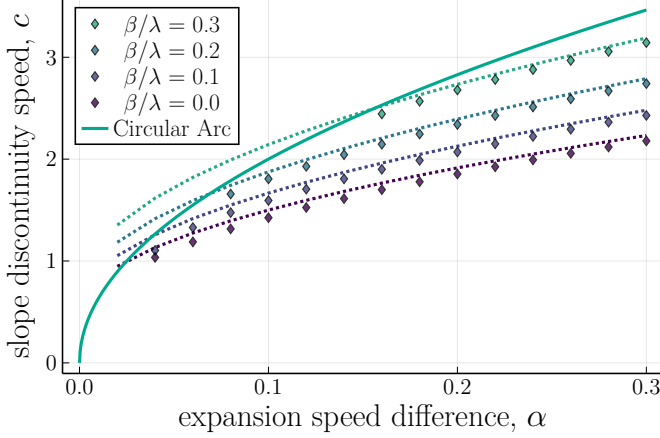


FIG. 5. The speed of the discontinuity in the slope is measured by tracking the point where  $h = 1.01v_0t$ , i.e. the front is one percent higher than the flat front. The solid blue line is the invasion speed of the circular arc morphology  $u_{kpz} = \sqrt{2\alpha\lambda}$ , and the dashed lines are the analytical results from combining Eqs. (14) and (15). The parameters are the same as Fig. 3.

and all of our results hold for this case provided we replace  $s_0$  by  $-s_0f_0$ , which is the effective fitness advantage in the limit of small  $f$  in the new model. For  $f_0 > -1/2$ , the traveling-wave solutions become pushed, i.e. their velocity depends not only on  $s(0)$ , which controls the dynamics at the invasion edge, but on the entire shape of  $s(f)$  because the competition across the entire invasion front contributes to the invasion velocity [28, 42–46].

Within the class of pushed wave, one typically distinguishes waves propagating into a metastable state ( $f_0 > 0$ ) and waves propagating into an unstable state ( $f_0 < 0$ ). In our previous work [16], we showed that these two subclasses of pushed waves behave differently at large negative  $\alpha$ . The former undergo a wave reversal with  $u$  becoming negative while the latter effectively become pulled, and the invasion velocity approaches  $2\sqrt{-s_0f_0D_f}$ . The same distinction holds for anisotropic growth without any modification, so our analysis below is primarily concerned with positive and slightly negative  $\alpha$  for which there are nontrivial effects of anisotropy.

To determine  $u$ , we treat the couplings between the KPZ and FKPP equations as perturbations. Hence, the unperturbed solution of Eq. (16) (with  $\beta$  set to zero) for the profile shape  $f^{(0)}(z)$  and invasion speed  $u_0$  are given by the classic results [27]:

$$f^{(0)} = \frac{1}{1 + e^{\sqrt{\frac{s_0}{2D_f}}z}}, \quad (17)$$

$$u_0 = \sqrt{\frac{s_0D_f}{2}}(1 - 2f_0). \quad (18)$$

We now use this zeroth order solution to determine the

shape of the colony  $h$  from Eq. (5). For a V-shaped dent and composite bulge this was done in Ref. [16], so we focus on the new morphology of an escaping bulge. Similar to our analysis of pulled waves, we first change into the reference frame co-moving with the sector boundary in both horizontal and vertical directions. The former is accomplished by defining  $z = x - ut$ , and the latter is achieved by the transformation  $h \rightarrow h + (v_0 + \alpha - u^2/(2\lambda))t$ , which results in the following equation for  $h$ :

$$-uh'(z) = \frac{u^2}{2\lambda} + \alpha(f^{(0)} - 1) + \frac{\lambda}{2}(h')^2 + D_h h''. \quad (19)$$

While Eq. (19) can be reduced to a Riccati equation, it is simpler and perhaps more informative to calculate the colony shape  $h$  in the limit of geometric optics by setting  $D_h = 0$ . We then obtain that

$$h'(z) = -\frac{u}{\lambda} - \sqrt{\frac{2\alpha}{\lambda}(1 - f^{(0)}(z))}, \quad (20)$$

which determines the coupling term in the FKPP equation. Thus, we have all the information necessary to compute the correction to  $u_0$  from the last term in Eq. (16). This is done by the standard perturbation theory for pushed waves [42–46] and results in

$$u = u_0 - \beta \frac{\int_{-\infty}^{\infty} h'(f^{(0)'})^2 e^{u_0 z/D_f} dz}{\int_{-\infty}^{\infty} (f^{(0)'})^2 e^{u_0 z/D_f} dz}. \quad (21)$$

For  $\beta = \lambda$ , we previously showed that this equation matches numerical solutions for  $\alpha$  not too different from zero [16]. This agreement persists for  $\beta \neq \lambda$  as long as  $\alpha$  is small enough not to create a circular arc or an escaping bulge (Fig. 6). Note that one must use  $h'$  for the V-dent and composite bulge morphologies derived in Ref. [16]. In fact, the only change that must be done in the previous calculation is the replacement of  $\lambda$  by  $\beta$  in front of the ratio of the integrals.

For an escaping bulge morphology of interest to us here, we substitute the approximate value for  $h'$  from Eq. (20) into Eq. (21) and find that

$$u = \frac{u_0 + \gamma \frac{\beta}{\lambda} \sqrt{2\alpha\lambda}}{1 - \frac{\beta}{\lambda}}, \quad (22)$$

where

$$\gamma = \frac{\int_{-\infty}^{\infty} \sqrt{1 - f^{(0)}}(f^{(0)'})^2 e^{u_0 z/D_f} dz}{\int_{-\infty}^{\infty} (f^{(0)'})^2 e^{u_0 z/D_f} dz}. \quad (23)$$

is a numerical factor, which depends on  $f_0$  and can in principle be evaluated analytically [47]. For  $f_0 \rightarrow -1/2$ , i.e. on the boundary with pulled waves  $\gamma \rightarrow 1$ , which indeed coincides with our results in the previous section. For larger values of  $f_0$ , this prefactor is strictly less than one, and  $\gamma \rightarrow 24/35$  as  $f_0 \rightarrow 1/2$ .



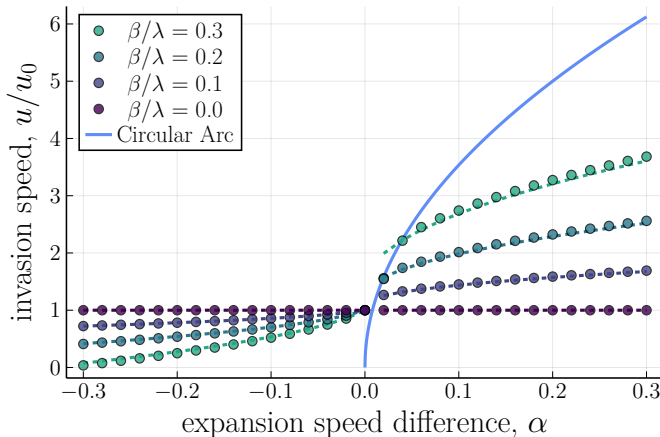


FIG. 6. **Invasion speed for pushed waves** (Color Online). The symbols are from numerical solution of Eqs. (5) and (16), and the dashed colored lines are the theoretical expectations. Three theoretical solutions are shown: the perturbative solution for a composite bulge and V-shaped dent, i.e. Eq. (21) (The ratio of integrals was approximated using Eq. 17 in the supplemental material of reference [16], giving  $\kappa = 0.51$ ), the circular arc solution with  $u = u_{\text{KPZ}} = \sqrt{2\alpha\lambda}$ , and the escaping bulge solution given by (22) (we used  $\gamma = 0.83$  obtained from Eq. (20)). Note that there is a fourth regime at large negative  $\alpha$  with  $u < 0$ , which describes the invasion of the ancestor; see Ref. [16] for more details. Parameters are:  $v_0 = 1$ ,  $\lambda = 20$ ,  $D_h = 1$ ,  $D_f = 1$ ,  $s_0 = 1$ , and  $f_0 = 0.1$ .

Equations (22) and (23), which were derived for  $D_h = 0$ , nevertheless match very well with our numerical results for  $D_h = 1$  shown in Fig. 6. The region of the parameter space that leads to an escaping bulge can be determined just as for pulled waves. Namely, we set the vertical velocity of the sector boundary to  $v_0$ , and find that an escaping bulge occurs only when  $u < u_{\text{KPZ}}$ . This condition can be fulfilled only when  $\beta < \lambda/(1 + \gamma)$ , which immediately follows from Eq. (22). Since  $\gamma$  is typically less than one for pushed waves, we conclude that an escaping bulge requires weaker anisotropy in pushed compared to pulled waves. The transitions among different morphologies for pushed waves with positive  $f_0$  are summarized in Fig. 7.

Finally, we note that all the calculations leading to Eq. (15) are geometric in nature and do not depend on whether the wave is pushed or pulled. So this result for the speed of the shock-like deformation of the front holds for pushed waves as well.

## DISCUSSION

We have considered a system of two coupled partial differential equations that describe one-dimensional reaction-diffusion waves and surface growth respectively. [15] A related geometric perspective was developed to understand novel sector morphologies observed

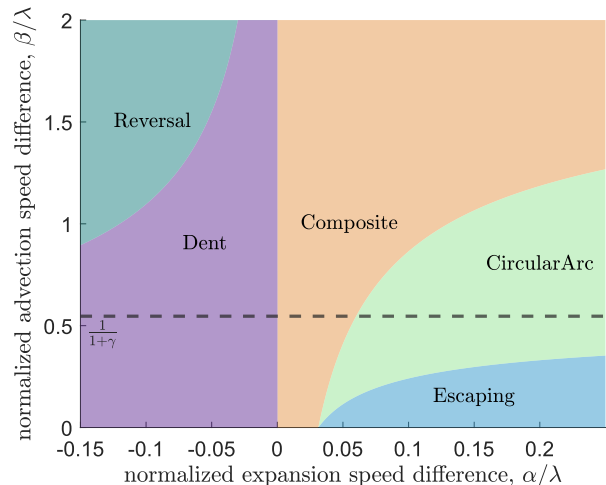


FIG. 7. **Predicted phase diagram of morphologies for pushed waves** (Color Online). The phase boundaries are obtained by matching the invasion speeds computed for the three morphologies as a function of the normalized expansion speed difference  $\alpha/\lambda$ , and the normalized anisotropy  $\beta/\lambda$ . In particular, the boundary between the composite bulge and the circular arc is determined by equating the natural KPZ velocity  $\sqrt{2\alpha\lambda}$  to  $u$  from Eqn. (21) as we did previously for isotropic growth [16]. The boundary between the circular arc and escaping bulge morphology is given by Eq. (22). Note that the escaping bulge morphology is only accessible for  $\beta < \lambda/(1 + \gamma)$ . For  $f_0 > 0$ , pushed waves also possess a “Reversal” phase where the direction of invasion flips due to an overwhelming growth rate disadvantage [16]. Here, parameters are  $u_0 = 1$ ,  $\lambda = 10$ , and  $\kappa = 0.51$ ,  $\gamma = 0.83$  corresponding to  $f_0 = 0.1$ .

in microbial colonies [8]. The equations (and hence their solutions) can also be mapped to other examples of expanding populations, such as a hydrodynamic model of competition under self-generated flow [48]. We studied this model previously under the constraint of rotational invariance in the context of colony growth, or Galilean invariance in the context of hydrodynamics [16]. Here, we explored the consequences of anisotropy and discovered a fundamentally new sector morphology. Taken together, our results established the phase diagram of sector shapes and determined the invasion velocity in each of the possible regimes.

While our analysis relied on somewhat technical methods including numerical simulations, perturbative calculations, and pattern selection criteria, we can also provide a simple intuition behind the main results. We found that, despite the two-way coupling, the KPZ and FKPP equations make nearly distinct contributions to the invasion dynamics. This distinction is particularly clear for pulled waves, so we discuss this case first.

For negative  $\alpha$ , the invasion velocity  $u$  and, therefore, the position of the sector boundary is controlled only by the FKPP equation. The sector morphology then



emerges from the KPZ equation with a source term that moves with velocity  $u$ , which is imposed externally to the KPZ equation. The solution of this driven KPZ equation is simply a straight line, which is bound by the sector boundary on the right and another straight line from the left-moving sector boundary on the left. After considering both edges, we recover the V-dent morphology.

These dynamics stay mostly the same as  $\alpha$  becomes positive. The invasion speed still emerges from the FKPP equations, and the sector morphology is dictated by a moving source in the KPZ equation. The solution of the driven KPZ equation is still a straight line, but now with a negative slope because  $\alpha > 0$ . This linear segment is again bounded by the sector boundary on the right. The dynamics on the left side, however, changes. Instead of a stationary slope discontinuity at the initial location of the mutant, the central region of the sector now consists of a circular arc [49]. This circular arc solution is only possible for  $\alpha > 0$  and represents the outward growth of a faster strain from its initial location. For small  $\alpha$ , the horizontal velocity of the circular arc,  $u_{\text{kpz}}$ , is smaller than the Fisher velocity, so the sector boundary is ahead of the point where the shape of the front transitions from a slope to a circular arc. Overall, this results in the morphology of a composite bulge.

As  $\alpha$  increases further, the velocity of the circular arc becomes larger than the Fisher velocity. At this point, the sector boundary and the transition from flat to circular front coincide and move with  $u_{\text{kpz}}$ . Thus, we recover the commonly observed circular bulge morphology. We note that in this regime, the invasion is controlled entirely by the KPZ dynamics and the FKPP equation simply ensures that the sector boundary keeps up with the circular arc. Indeed, the advection term from the coupling to  $h$  vanishes ahead of the circular arc, but results in a substantial advection velocity behind the circular arc. For nearly isotropic case  $\beta \approx \lambda$ , this advection velocity is sufficient for the mutant strain to keep with the circular arc even if  $s_0 \rightarrow 0$ .

The situation changes for  $\beta < \lambda/2$  because the advection velocity, which is linear in  $\beta$ , is no longer sufficient to keep up with the circular arc. So, for large enough  $\alpha$ , the combined Fisher and advection velocities become smaller than the velocity of the circular arc. The sector boundary then falls behind the transition point to the flat front thereby producing an escaping bulge morphology. In this regime, the sector boundary and the shock-like singularity move with different velocities:  $u$  and  $c$  respectively. The values of these velocities receive equal contributions for the KPZ and FKPP equations (Eqs. (15) and (22)), unlike in the other three regimes in which only one of the two equations controls the dynamics. Perhaps the chief reason for this difference is the fact that the sector boundary is now entirely located in a region with nonzero slope.

Pushed waves follow the same transitions as  $\alpha$  increases

from negative to positive values except that the invasion velocity  $u$  does depend on  $\alpha$  for the V-shaped dent and the composite bulge because  $\partial h/\partial x \neq 0$  for the bulk of the lateral invasion front in the FKPP equation. As a result, the transitions between different morphologies are determined by the relative values of  $u$  and  $u_{\text{kpz}}$  rather than the Fisher velocity and  $u_{\text{kpz}}$ .

In summary, we have characterized the effects of anisotropy on the patterns of spatial competition during range expansions. Weak anisotropy has no effect on population dynamics for pulled waves and results in only quantitative changes for pushed waves. Therefore, the detection of anisotropy from sector patterns may be either impossible or require very precise measurements. Strong anisotropy, however, can create a distinct spatial pattern with a shock-like deformation ahead of the sector boundary. The emergence of this pattern could thus provide a useful signature of anisotropic growth in future studies.

## ACKNOWLEDGEMENTS

D.S. acknowledges support from the MathWorks School of Science Fellowship. H.L. acknowledges support from the Sloan Foundation through grant G-2021-16758. M.K. acknowledges support from NSF through grant DMR-2218849. K.S.K. was supported by the NIGMS grant 1R01GM138530-01.

- 
- [1] B. Joyce, Molecular beam epitaxy, Reports on Progress in Physics **48**, 1637 (1985).
  - [2] J. Hirschfelder and C. Curtiss, The theory of flame propagation, The Journal of Chemical Physics **17**, 1076 (1949).
  - [3] N. S. Dhillon, J. Buongiorno, and K. K. Varanasi, Critical heat flux maxima during boiling crisis on textured surfaces, Nature communications **6**, 8247 (2015).
  - [4] J. D. Murray, *Mathematical biology: I. An introduction* (Springer, 2002).
  - [5] O. Hallatschek, P. Hersen, S. Ramanathan, and D. R. Nelson, Genetic drift at expanding frontiers promotes gene segregation, Proceedings of the National Academy of Sciences **104**, 19926 (2007).
  - [6] K. S. Korolev, Evolution arrests invasions of cooperative populations, Physical review letters **115**, 208104 (2015).
  - [7] A. Plummer, R. Benzi, D. R. Nelson, and F. Toschi, Fixation probabilities in weakly compressible fluid flows, Proceedings of the National Academy of Sciences **116**, 373 (2019).
  - [8] H. Lee, J. Gore, and K. S. Korolev, Slow expanders invade by forming dented fronts in microbial colonies, Proceedings of the National Academy of Sciences **119**, e2108653119 (2022).
  - [9] M. Gralka, F. Stiewe, F. Farrell, W. Möbius, B. Walclaw, and O. Hallatschek, Allele surfing promotes micro-

- bial adaptation from standing variation, *Ecology letters* **19**, 889 (2016).
- [10] R. Jullien and R. Botet, Scaling properties of the surface of the eden model in  $d = 2, 3, 4$ , *Journal of Physics A: Mathematical and general* **18**, 2279 (1985).
  - [11] K. S. Korolev, M. Avlund, O. Hallatschek, and D. R. Nelson, Genetic demixing and evolution in linear stepping stone models, *Reviews of modern physics* **82**, 1691 (2010).
  - [12] M. Kardar, G. Parisi, and Y.-C. Zhang, Dynamic scaling of growing interfaces, *Physical Review Letters* **56**, 889 (1986).
  - [13] R. A. Fisher, The wave of advance of advantageous genes, *Annals of eugenics* **7**, 355 (1937).
  - [14] A. Kolmogorov, I. Petrovskii, and N. Piskunov, *Moscow university bull* (1937).
  - [15] J. M. Horowitz and M. Kardar, Bacterial range expansions on a growing front: Roughness, fixation, and directed percolation, *Physical Review E* **99**, 042134 (2019).
  - [16] D. W. Swartz, H. Lee, M. Kardar, and K. S. Korolev, Interplay between morphology and competition in two-dimensional colony expansion, *Physical Review E* **108**, L032301 (2023).
  - [17] K. S. Korolev, M. J. Müller, N. Karahan, A. W. Murray, O. Hallatschek, and D. R. Nelson, Selective sweeps in growing microbial colonies, *Physical biology* **9**, 026008 (2012).
  - [18] H. L. de Barros, D. Esquivel, and M. Farina, Magnetotaxis, *Science Progress* (1933-) , 347 (1990).
  - [19] R. Angel, M. I. M. Soares, E. D. Ungar, and O. Gillor, Biogeography of soil archaea and bacteria along a steep precipitation gradient, *The ISME journal* **4**, 553 (2010).
  - [20] A. Dewle, N. Pathak, P. Rakshasmar, and A. Srivastava, Multifarious fabrication approaches of producing aligned collagen scaffolds for tissue engineering applications, *ACS Biomaterials Science & Engineering* **6**, 779 (2020).
  - [21] M. Parsa, S. Harmand, K. Sefiane, M. Biggerelle, and R. Deltombe, Effect of substrate temperature on pattern formation of nanoparticles from volatile drops, *Langmuir* **31**, 3354 (2015).
  - [22] A. Giometto, D. R. Nelson, and A. W. Murray, Physical interactions reduce the power of natural selection in growing yeast colonies, *Proceedings of the National Academy of Sciences* **115**, 11448 (2018), publisher: Proceedings of the National Academy of Sciences.
  - [23] J. Kayser, C. F. Schreck, M. Gralka, D. Fusco, and O. Hallatschek, Collective motion conceals fitness differences in crowded cellular populations, *Nature ecology & evolution* **3**, 125 (2019).
  - [24] O. Hallatschek and D. R. Nelson, Life at the Front of an Expanding Population, *Evolution* **64**, 193 (2010), eprint: <https://onlinelibrary.wiley.com/doi/pdf/10.1111/j.1558-5646.2009.00809.x>.
  - [25] F. Beroz, J. Yan, Y. Meir, B. Sabass, H. A. Stone, B. L. Bassler, and N. S. Wingreen, Verticalization of bacterial biofilms, *Nature physics* **14**, 954 (2018).
  - [26] L. Roques, J. Garnier, F. Hamel, and E. K. Klein, Allee effect promotes diversity in traveling waves of colonization, *Proceedings of the National Academy of Sciences* **109**, 8828 (2012).
  - [27] P. C. Fife and J. B. McLeod, The approach of solutions of nonlinear diffusion equations to travelling front solutions, *Archive for Rational Mechanics and Analysis* **65**, 335 (1977).
  - [28] W. Van Saarloos, Front propagation into unstable states, *Physics reports* **386**, 29 (2003).
  - [29] T. Storck, C. Picioreanu, B. Virdis, and D. J. Batstone, Variable cell morphology approach for individual-based modeling of microbial communities, *Biophysical journal* **106**, 2037 (2014).
  - [30] B. Drossel and M. Kardar, Phase ordering and roughening on growing films, *Physical Review Letters* **85**, 614 (2000).
  - [31] A. B. George and K. S. Korolev, Chirality provides a direct fitness advantage and facilitates intermixing in cellular aggregates, *PLOS Computational Biology* **14**, e1006645 (2018), publisher: Public Library of Science.
  - [32] D. R. Nelson and N. M. Shnerb, Non-hermitian localization and population biology, *Physical Review E* **58**, 1383 (1998).
  - [33] O. M. Ghosh and B. H. Good, Emergent evolutionary forces in spatial models of luminal growth and their application to the human gut microbiota, *Proceedings of the National Academy of Sciences* **119**, e2114931119 (2022).
  - [34] We note in passing the the breaking of the rotational symmetry in the coupled KPZ-FKPP equations corresponds to the breaking of Galilean invariance in the coupled Burgers-FKPP equations.
  - [35] F. Montel, M. Delarue, J. Elgeti, D. Vignjevic, G. Cappello, J. Prost, and J.-F. Joanny, Stress clamp experiments on multicellular tumor spheroids, *Biophysical Journal* **102**, 220a (2012).
  - [36] L. Dai, D. Vorselen, K. S. Korolev, and J. Gore, Generic indicators for loss of resilience before a tipping point leading to population collapse, *Science* **336**, 1175 (2012).
  - [37] S. R. Gandhi, E. A. Yurtsev, K. S. Korolev, and J. Gore, Range expansions transition from pulled to pushed waves as growth becomes more cooperative in an experimental microbial population, *Proceedings of the National Academy of Sciences* **113**, 6922 (2016).
  - [38] R. Menon and K. S. Korolev, Public good diffusion limits microbial mutualism, *Physical review letters* **114**, 168102 (2015).
  - [39] M. O. Lavrentovich and D. R. Nelson, Asymmetric mutualism in two-and three-dimensional range expansions, *Physical review letters* **112**, 138102 (2014).
  - [40] C. D. Nadell, K. Drescher, and K. R. Foster, Spatial structure, cooperation and competition in biofilms, *Nature Reviews Microbiology* **14**, 589 (2016).
  - [41] K. Korolev and D. R. Nelson, Competition and cooperation in one-dimensional stepping-stone models, *Physical Review Letters* **107**, 088103 (2011).
  - [42] G. Birzu, O. Hallatschek, and K. S. Korolev, Fluctuations uncover a distinct class of traveling waves, *Proceedings of the National Academy of Sciences* **115**, E3645 (2018), publisher: Proceedings of the National Academy of Sciences.
  - [43] B. Meerson, P. V. Sasorov, and Y. Kaplan, Velocity fluctuations of population fronts propagating into metastable states, *Physical Review E* **84**, 011147 (2011).
  - [44] G. Paquette, L.-Y. Chen, N. Goldenfeld, and Y. Oono, Structural stability and renormalization group for propagating fronts, *Physical review letters* **72**, 76 (1994).
  - [45] A. Rocco, J. Casademunt, U. Ebert, and W. van Saarloos, Diffusion coefficient of propagating fronts with multiplicative noise, *Physical Review E* **65**, 012102 (2001).
  - [46] A. Mikhailov, L. Schimansky-Geier, and W. Ebeling, Stochastic motion of the propagating front in bistable

- media, Physics Letters A **96**, 453 (1983).
- [47] It is easy to show that only the equation for  $\gamma$  is affected by our approximation that  $D_h = 0$  while the equation for  $u$  is valid for  $D_h > 0$  as well.
- [48] R. Alert, J. Casademunt, and J.-F. Joanny, Active turbulence, Annual Review of Condensed Matter Physics **13**, 143 (2022).
- [49] Technically a parabolic segment, which is equivalent to a circle in the limit of small spatial gradients of  $h$ .